HHS Public Access

Author manuscript

Int J Cancer. Author manuscript; available in PMC 2024 September 01.

Published in final edited form as:

Int J Cancer. 2023 September 01; 153(5): 1051–1066. doi:10.1002/ijc.34564.

Genetic deletion or tyrosine phosphatase inhibition of PTPRZ1 activates c-Met to up-regulate angiogenesis and lung adenocarcinoma growth

Pinelopi Kastana[1,#], **Despoina Ntenekou**[1,#], **Eleni Mourkogianni**[1,$], **Michaela-Karina Enake**[1,$], **Athanasios Xanthopoulos**[1], **Effrosyni Choleva**[1], **Antonia Marazioti**[2,¥], **Sophia Nikou**[3], **Racheal G. Akwii**[4], **Eleni Papadaki**[3], **Esther Gramage**[5], **Gonzalo Herradón**[5], **Georgios T. Stathopoulos**[2,@], **Constantinos M. Mikelis**[1,4], **Evangelia Papadimitriou**[1,*]

[1]Laboratory of Molecular Pharmacology, Department of Pharmacy, University of Patras, Greece

[2]Laboratory of Molecular Respiratory Carcinogenesis, Department of Physiology, Faculty of Medicine, University of Patras, Greece

[3]Department of Anatomy, Faculty of Medicine, University of Patras, Greece

[4]Department of Pharmaceutical Sciences, School of Pharmacy, Texas Tech University Health Sciences Centre, Amarillo, TX, USA

[5]Departamento de Ciencias Farmacéuticas y de la Salud, Facultad de Farmacia, Universidad San Pablo-CEU, CEU Universities, Madrid, Spain

Abstract

Protein tyrosine phosphatase receptor zeta 1 (PTPRZ1) is a transmembrane tyrosine phosphatase (TP) expressed in endothelial cells and required for stimulation of cell migration by vascular endothelial growth factor A_{165} ($VEGFA_{165}$) and pleiotrophin (PTN). It is also over or under-expressed in various tumor types. In this study, we used genetically engineered *Ptprz1*$^{-/-}$

[*]C**orrespondence**: Evangelia Papadimitriou, Ph.D., Laboratory of Molecular Pharmacology, Department of Pharmacy, University of Patras, GR 26504 Patras, Greece. Tel: 0030-2610-962336, epapad@upatras.gr.

[#], [$]These authors equally contributed to the work

[¥]Current address: Laboratory of Basic Sciences, Department of Physiotherapy, School of Health Sciences, University of Peloponnese, Greece 23100

[@]Current address: Comprehensive Pneumology Center (CPC) and Institute for Lung Biology and Disease (iLBD); Helmholtz Center Munich-German Research Center for Environmental Health (HMGU); Munich, Bavaria, 81377; Germany

Authors' contributions

The authors have performed the work reported in the paper, except for RNA sequencing and bioinformatics analysis, as described. PK, DNt, EM, M-KE, AX, EC, AM, SN, RGA, and EG performed experiments and/or analyzed data; GH, ElP, GTS, CMM, and EvP supervised experiments and analyzed data; PK, DNt, and EvP designed the study and drafted the manuscript; EvP wrote the manuscript; all authors read and revised the manuscript.

Conflict of interest

Part of these data has been included in a patent: Papadimitriou E, Kastana P & Ntenekou D. *Methods for determining the prognosis of a subject with lung adenocarcinoma and responsiveness to treatment*. Hellenic Industrial Property Organization Patent No: 1010022/01.06.2021 (Patent Application No. 20200100138/17.03.2020). All other authors declare no conflict of interest.

Ethics Statement

All animal experiments were designed and approved *a priori* by the Veterinary Administration of the Prefecture of Western Greece (approval protocol numbers 108269/428/28-4-2017 and 388223/1166/8-1-2020), according to Directive 2010/63/EU (http://eurlex.europa.eu/legal-content/EN/TXT/?uri=CELEX%3A32010L0063). All procedures performed in studies involving HUVEC were under the ethical standards of the institutional research committee (Bioethics Committee of the University of Patras) and with the 1964 Helsinki Declaration and its later amendments or comparable ethical standards.

and *Ptprz1*$^{+/+}$ mice to study mechanistic aspects of PTPRZ1 involvement in angiogenesis and investigate its role in lung adenocarcinoma (LUAD) growth. *Ptprz1*$^{-/-}$ lung microvascular endothelial cells (LMVEC) have increased angiogenic features compared to *Ptprz1*$^{+/+}$ LMVEC, in line with the increased lung angiogenesis and the enhanced chemically induced LUAD growth in *Ptprz1*$^{-/-}$ compared to *Ptprz1*$^{+/+}$ mice. In LUAD cells isolated from the lungs of urethane-treated mice, PTPRZ1 TP inhibition also enhanced proliferation and migration. Expression of beta 3 (β_3) integrin is decreased in *Ptprz1*$^{-/-}$ LMVEC, linked to enhanced VEGF receptor 2 (VEGFR2), c-Met tyrosine kinase (TK), and Akt kinase activities. However, only c-Met and Akt seem responsible for the enhanced endothelial and cell activation *in vitro* and LUAD growth and angiogenesis *in vivo* in *Ptprz1*$^{-/-}$ mice. A selective PTPRZ1 TP inhibitor, $VEGFA_{165}$, and PTN also activate c-Met and Akt in a PTPRZ1-dependent manner in endothelial cells, and their stimulatory effects are abolished by the c-Met TK inhibitor (TKI) crizotinib. Altogether, our data suggest that low PTPRZ1 expression is linked to worse LUAD prognosis and response to c-Met TKIs and uncover for the first time the role of PTPRZ1 in mediating c-Met activation by VEGFA and PTN.

Graphical Abstract

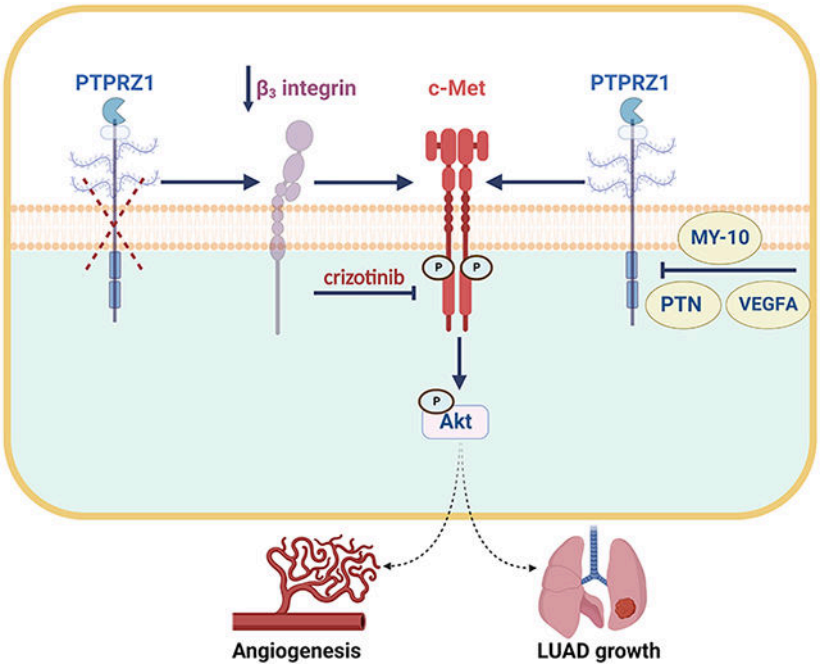

Keywords

endothelial cells; hepatocyte growth factor receptor; integrin; pleiotrophin; VEGFA

1. Introduction

Protein tyrosine phosphatase receptor zeta 1 (PTPRZ1) is a transmembrane tyrosine phosphatase (TP) with high expression in fetal cells or during embryonic development, and low systemic expression in the adult [1]. PTPRZ1 expression is significantly altered in

several types of cancer. It is overexpressed in glioblastoma stem cells, seems to be important for glioblastoma growth [1, 2], and contributes to resistance to temozolomide [3]. Similarly, in neuroendocrine small-cell lung carcinoma, overexpression of PTPRZ1 seems to promote tumor progression [4]. On the other hand, in prostate cancer [5] and osteosarcoma [6], PTPRZ1 expression is decreased and inversely correlates with cancer progression. In ovarian cancer, the decreased PTPRZ1 expression seems to be related to resistance to cisplatin [7]. In lung adenocarcinoma (LUAD), based on TCGA data, PTPRZ1 gene expression inversely correlates to patient overall survival [8]; however, there are no data on the role of PTPRZ1 in LUAD growth *in vitro* or *in vivo*.

PTPRZ1 ligands are pleiotrophin (PTN), midkine, fibroblast growth factor 2, interleukin-34, and vascular endothelial growth factor A (VEGFA). In most cases, ligand binding to PTPRZ1 has been reported to inactivate its TP activity, leading to the activation of numerous downstream signaling molecules, such as Src family kinases and phosphoinositide 3-kinase (reviewed in [1, 8]). PTPRZ1 is expressed in endothelial cells *in vitro* and is required for both PTN- and $VEGFA_{165}$-induced cell migration [9, 10]. It also mediates the stimulatory effect of $VEGFA_{165}$ on cell surface nucleolin localization [10] and its inhibitory effect on PTN expression [11]. Both these activities seem to be independent of VEGF receptor 2 (VEGFR2) [10, 11], suggesting that PTPRZ1 warrants further investigation as a potential novel target that will contribute to overcoming the resistance to the existing anti-angiogenic therapies that inhibit the interaction or the signaling of VEGFA through VEGFR2 [12], thus improving patient survival.

In the present work, the role of PTPRZ1 expression in physiological angiogenesis, as well as in LUAD angiogenesis and growth was studied *in vivo*, using genetically engineered *Ptprz1*$^{-/-}$ and *Ptprz1*$^{+/+}$ mice. Endothelial cells isolated from the lungs of these mice were used to study mechanistic aspects of the involvement of PTPRZ1 in endothelial cell functions *in vitro*. LUAD cells isolated from the lungs of urethane-treated mice were used to study the role of PTPRZ1 on their proliferation and migration *in vitro*. Our data suggest that PTPRZ1 deletion significantly enhances endothelial cell functions and angiogenesis through decreased β_3 integrin expression and activation of c-Met and Akt. Our data uncover for the first time a role of PTPRZ1 in mediating c-Met activation, highlight the role of PTPRZ1 in PTN- and VEGFA-induced c-Met activation and signaling in endothelial cells, suggest a potential role of PTPRZ1 in LUAD growth and show evidence for the antiangiogenic effects of existing c-Met TK inhibitors (TKIs). They also propose the potential use of PTPRZ1 as a prognostic and predictive biomarker for LUAD patients that could benefit from c-Met TKIs.

2. Materials and Methods

2.1 Mice

The *Ptprz1*$^{-/-}$ mice (SV129/B6 strain) were produced by Dr. Sheila Harroch, Institut Pasteur, France [13] and were kindly provided to us by Dr. Heather Himburg and Prof. John Chute at UCLA, USA. The animals were bred at the Centre for Animal Models of Disease at the University of Patras, Greece (EL13B1004), in a controlled environment of 12 h light/dark cycles and food/water consumption *ad libitum*. *Ptprz1*$^{-/-}$ mice have no obvious

phenotype related to general development, behavior, breeding, or survival compared to the corresponding *Ptprz1*$^{+/+}$ mice, as previously reported [13].

2.2 Cell culture

For lung microvascular endothelial cell (LMVEC) isolation, 2-5 mice were humanely euthanized between 3-8 weeks of age by exposure to CO_2 levels greater than 70% for 5 min. The lungs were immediately harvested, minced in 1 ml DMEM, and incubated in DMEM containing 0.2% Gibco® Collagenase Type I (ThermoFisher Scientific; #17018029) for 4 h at 37°C. The cell-tissue suspension was serially filtered through 140 μm and 60 μm filters, the filtrate was centrifuged at 500 g for 5 min at room temperature (RT) and the cell pellet was resuspended and cultured [14]. Endothelial cells were purified using Dynabeads™ CD31 Endothelial Cell (Thermo Fisher Scientific; #11155D), following the manufacturer's instructions, and purity was verified by *Griffonia simplicifolia* staining, as described below. HUVEC were isolated as previously described [9, 10]. LMVEC and HUVEC were cultured in DMEM low glucose supplemented with 15% fetal bovine serum (FBS), 150 g/ml endothelial cell growth supplement, 5 units/ml heparin sodium, 100 units/ml penicillin/streptomycin, and 2.5 μg/ml amphotericin B.

Primary lung adenocarcinoma cells from FVB mice (FULA cells) were generated as described elsewhere [15, 16]. Briefly, FVB mice received repetitive intraperitoneal urethane injections and were observed for 9 months for true lung adenocarcinoma to develop. Mice developed large tumors that were harvested under sterile conditions, minced, passed through a 100 μm-strainer, and cultured separately in DMEM high glucose containing 10% FBS, 100 units/ml penicillin/streptomycin, and 2.5 μg/ml amphotericin B. These cells were fully characterized for their malignant nature *in vitro* and *in vivo* [16]. All cells were maintained at 37°C, 5% CO_2, and 100% humidity. All experiments were performed with mycoplasma-free cells.

2.3 Proliferation assay

LMVEC were plated in 48-well plates (1.5 x 10^4 cells/well) and at different time points after plating, cells were harvested by trypsin and counted using a hemocytometer. The selective PTPRZ1 TP inhibitor MY10 (10 μM) [17], the VEGFR2 specific inhibitor SU1498 (10 μM, Santa Cruz Biotechnology, Inc., #sc-474570) or the c-Met inhibitor crizotinib (1 μM, TargetMol, Boston, MA, USA; #T1661) were added in the culture medium 24 h after plating. HUVEC were plated in 48-well plates (2.5 x 10^4 cells/well) and 24 h after plating, serum-starved overnight, and then treated with $VEGFA_{165}$ (10 ng/ml) in the presence or absence of crizotinib for 24 h.

2.4 Migration assay

We used 24-well micro chemotaxis chambers (Corning, Glendale, AZ, USA; #3422) with uncoated polycarbonate membranes with 8 μm pores. The bottom chamber was filled with 0.6 ml of serum-free medium containing 0.25% bovine serum albumin (BSA) in the presence of the tested agents or the corresponding solvent. Harvested cells were resuspended at a concentration of 10^5 cells/0.1 ml serum-free medium containing 0.25% BSA, loaded in the upper chamber of the transwell, and the whole transwell system was incubated for 4 h at

37°C. Filters were fixed with Carson's phosphate-buffered paraformaldehyde for 10 min and stained with 0.33% toluidine blue solution. The cells that migrated through the filters were quantified in a blinded manner at the entire area of each filter by direct measurement on a light microscope (Optech Microscope Services Ltd.) [9, 10].

2.5 *In vitro* Matrigel assay

Growth factor reduced Matrigel™ (BD Matrigel™ Basement Membrane Matrix Growth Factor Reduced; BD Biosciences, San Jose, CA, USA; #354234) was added (0.05 ml) in each well of 96-well plates at 4°C and was left at 37°C for 1 h to solidify. LMVEC (2 x 10^4 cells in 0.1 ml of medium) were added in each well in the presence of the tested agents or the corresponding solvent. The tubes formed after 4 h of incubation at 37°C were photographed under an inverted Olympus IMT-2 microscope (Olympus Corporation, Japan) using a C-B3 camera (Optica Microscopy, Italy). The total length of the tube network was quantified in the total area of the wells using ImageJ, as previously described [9].

2.6 Immunofluorescence

Cells were fixed with 4% formaldehyde in PBS pH 7.4 for 10 min and permeabilized with PBS containing 0.1% Triton. Following blocking with PBS containing 3% BSA and 10% FBS for 1 h at RT, cells were incubated with a) mouse anti-PTPRZ1 (BD Biosciences; #610180) antibody at a 1:250 dilution followed by fluorescent 594 anti-mouse IgG secondary antibody (Molecular Probes, Carlsbad, CA) used at 1:500 dilution, or b) lectin solution (Rhodamine *Griffonia simplicifolia* lectin I, Vector Laboratories, Burlingame, CA, USA; #RL-1102) 1:800 in PBS pH 7.4 for 1 h at RT in the dark, followed by three washes with PBS. Nuclei were stained with Draq5 (Biostatus Limited, Leicestershire, UK; #DRS1000) at a final concentration of 3.3 μM in PBS pH 7.4, and cells were mounted with Mowiol 4–88 (Sigma-Aldrich, St. Louis, MO, USA; #81381) and visualized at RT with a Leica SP5 (40x objective) confocal microscope.

2.7 Proximity ligation assay (PLA)

Cells: 4 x 10^4 or 1.2 x 10^4 LMVEC or HUVEC were seeded per coverslip in a 24-well plate or per well in a 12-well slide (Ibidi, #81201), respectively. When cells reached 80% confluency, they were either processed directly, treated with SU1498 (10 μM) or crizotinib (1 μM) for 2 h, or serum-starved for 16 h and then treated with SU1498 or crizotinib for 30 min and stimulated with MY10 (10 μM), $VEGFA_{165}$ (10 ng/ml) or PTN (100 ng/ml) for 10 min. Following fixation with 4% formaldehyde in PBS for 10 min at RT and permeabilization with 0.05% Triton X-100 in PBS for 5 min at RT, *in-situ* PLAs were performed with the following assay kits from Navinci (Uppsala, Sweden): Naveni pY Met for detection of tyrosine-phosphorylated c-Met, and Naveni pY VEGFR2 for detection of tyrosine-phosphorylated VEGFR2, according to the manufacturer's instructions. *Tissues*: Four μm thick LUAD tissue sections were deparaffinized in xylene and rehydrated in graded ethanol series (100%, 96%, 80%, 50%), followed by treatment with sodium citrate buffer (pH 6.0) for antigen retrieval. Tissue sections were permeabilized with 0.4% Triton X-100 in PBS supplemented with 1% FBS for 20 min (2 x 10 min) at RT. *In-situ* PLA for the detection of tyrosine-phosphorylated c-Met was performed using Naveni pY Met. In both cells and tissues, nuclei were stained with Draq5, as above. Cells/tissue sections were

mounted with Mowiol 4–88 and visualized at RT with Leica SP5 (40x objective) confocal microscope.

2.8 RNA isolation, RNA sequencing, and bioinformatics analysis

Total RNA was extracted from LMVEC using the NucleoSpin RNA Plus kit (Macherey-Nagel, Clonetech, CA, USA; # 740984.50). RNA concentration, purity, and integrity were estimated by using a Thermo Scientific™ NanoDrop™ One Microvolume UV-Vis Spectrophotometer, agarose gel electrophoresis, and the Agilent 2100 Bioanalyzer system. RNA from three independent isolations of the *Ptprz1*$^{+/+}$ and the *Ptprz1*$^{-/-}$ LMVEC was used for RNAseq analysis by Novogene Co., Ltd using an Illumina NovaSeq 6000 platform. Novogene also performed the bioinformatics analysis. For more details see Supplementary Methods. The sequencing coverage and quality statistics for each sample are summarized in Table S1.

2.9 RNA interference

LMVEC were grown to 40% confluence in a medium without antibiotics. Transfection was performed in serum-free medium for 4 h using annealed RNA for β_3 at the concentration of 33 nM (Santa Cruz Biotechnology, Inc., #sc-35677) in FBS-containing medium without antibiotics and Lipofectamine® RNAiMAX (Thermo Fisher Scientific; #13778075) as transfection reagent. Double-stranded negative control siRNA (Ambion, Austin, TX, USA) was used in all experiments. Cells were incubated for another 48 h in a serum-containing medium and fixed, lysed, or serum-starved before further experiments.

2.10 Urethane-induced carcinogenesis

The mice were sex, weight (17-20 g), and age (6 weeks) matched. No gender effect was observed. Lung carcinogenesis was chemically induced by 8 consecutive weekly intraperitoneal (i.p.) injections of freshly dissolved urethane (ethyl carbamate; Sigma-Aldrich; #U2500) at 1 g/kg in 0.9% NaCl [18, 19]. Crizotinib was dissolved in 30% PEG300, 5% DMSO, and 0.9% NaCl (solvent). Mice received weekly i.p. injections of crizotinib (25 mg/kg) or the solvent for 11 consecutive weeks, starting on week 3 after the first urethane injection. Crizotinib or solvent injections were performed one day after each urethane injection. At the end of the experiments, mice were humanely sacrificed by excessive CO_2 and head decapitation, in compliance with the Guide for the Care and Use of Laboratory Animals, and the lungs were extracted, filled with 10% formalin, and left overnight to be fixed. The tumors were counted blindly by two independent researchers and the diameter of each tumor was assessed using a Stemi DV4 stereoscope (Zeiss; Jena, Germany) with a micrometric scale incorporated into one eyepiece and an Axiocam ERc5s camera for photographs (Zeiss, Jena, Germany). Each tumor was considered as a sphere and its volume was calculated by using the equation $\pi\delta^3/6$. Tumor volume per animal was calculated by averaging individual tumor volumes per animal. Tumor burden was calculated as the sum of the tumor volumes per animal [19].

2.11 Histology/Immunohistochemistry

The lungs and tumors were fixed with 10% formalin and were paraffin-embedded. Four μm thick lung sections were cut and stained with eosin/hematoxylin (H&E). The tumor stage was scored in a blinded manner on a scale of 1 to 5, based on predetermined criteria, with 1 indicating the less advanced tumor phenotype [20]. For immunohistochemistry, the sections were deparaffinized, treated with EDTA for antigen retrieval, blocked with 2% BSA in PBS pH 7.4 for 15 min at RT, and incubated with the anti-macrophage primary antibody anti-rabbit macrophage concentrate mouse monoclonal, clone RAM11 (Agilent, Santa Clara, CA, USA; #M0633) at 1:50 dilution, the anti-PCNA rabbit polyclonal antibody (Abcam, Cambridge, UK; #ab2426) at 1:80 dilution, or the anti-PTPζ rabbit polyclonal antibody (Santa Cruz Biotechnology, #sc-25432) at 1:50 dilution, overnight at 4°C, followed by the Envision detection kit (Dako, #K4065). Hematoxylin was used for counterstaining. Photos were obtained under a microscope (Optech Microscope Services Ltd., Thames, UK) at 4, 10, 20, or 40x objectives. When needed, the number of stained and total cells per field was counted blindly by 2 different researchers in 2-3 different fields from each animal and results are expressed as the percent of stained cells per field.

In the case of staining tissue sections with *Griffonia simplicifolia*, following deparaffinization, the sections were washed three times with PBS pH 7.4, blocked with 2% BSA in PBS for 15 min at RT and incubated with a lectin solution diluted 1:200 in PBS, for 1 h at RT in the dark, followed by 3 washes with PBS. Nuclei were stained with Draq5 as described above and samples were mounted with Mowiol 4–88 and visualized at RT with Leica SP5 (63x objective) confocal microscope. The lectin-positive endothelial cells per field were quantified in 2-4 different fields from each animal using ImageJ, normalized with the tissue area and expressed as the vascularized area in arbitrary units (AU) [21].

2.12 Western blot analysis

Total protein cell/tissue lysates were analyzed by SDS-PAGE and transferred to PVDF membranes (Amersham™ Hybond® P Western blotting membranes, #GE10600023 or Porablot PVDF membrane, Macherey-Nagel, # 741260). Membranes were incubated with Tris-buffered saline (TBS), pH 7.4, with 0.05% Tween (TBS-T) containing either 5% non-fat dry milk or 3% BSA for 2 h at RT, washed 3 times with TBS-T, incubated with primary antibodies for 16 h at 4°C under continuous agitation, washed 3 times with TBS-T, and finally incubated with HRP-conjugated secondary antibodies (1:5000) for 1 h at RT. Primary antibodies used were mouse anti-PTPRZ1 (1:500, BD Biosciences; #610180), rabbit anti-phospho-Akt (Ser 473) and rabbit anti-Akt (1:1000, Cell Signaling Technology; #9271 and #9272), rabbit phospho-p44/42 MAPK and p44/p42 MAPK (1:1000, Cell Signaling Technology, #9101 and 9102), mouse anti-VEGFA (1:1000, Santa Cruz Biotechnology, #sc-7269), mouse anti-VEGFR2 (1:1000, Santa Cruz Biotechnology, #sc-6251), rabbit anti-VEGFR2 (1:1000, Cell Signaling Technology, #9698), rabbit phospho-VEGF Receptor 2 (Tyr1175) (1:500, Cell Signaling Technology, #2478), mouse anti-β3 integrin (1:1000, Santa Cruz Biotechnology, #sc-365679), mouse anti-Met (1:1000, Santa Cruz Biotechnology, #sc-8057), rabbit anti-vinculin (1:1000, Santa Cruz Biotechnology, #sc-5573) and mouse anti-beta actin (1:2000, Santa Cruz Biotechnology, #sc-58673). The HRP-conjugated secondary antibodies used were mouse anti-rabbit IgG-HRP (Santa Cruz Biotechnology,

Inc.; #sc-2357), m-IgGκ BP-HRP (Santa Cruz Biotechnology, Inc.; #sc-516102), anti-mouse IgG (Cell Signaling Technology; #7076), or anti-rabbit IgG (Cell Signaling Technology; #7074). Detection of immunoreactive bands was performed using the SuperSignal West Pico PLUS detection kit (Thermo Fisher Scientific, #34577). The protein levels that corresponded to each immunoreactive band were quantified using ImageJ.

2.13 Statistical Analysis

Unless otherwise indicated, data are expressed as mean ± SD from at least three independent assays performed in duplicates or triplicates. Student's unpaired t-test or one-way ANOVA analysis were performed to compare values between two or more two groups, respectively. Bullets in graphs represent independent assays (*in vitro*) or different mice (*in vivo*).

3. Results

3.1 PTPRZ1 deletion enhances angiogenic properties of LMVEC *in vitro* and physiological angiogenesis *in vivo*

LMVEC from *Ptprz1*$^{-/-}$ and *Ptprz1*$^{+/+}$ mice were isolated, cultured, and tested for endothelial cell markers and PTPRZ1 expression (Fig. 1A). Proliferation (Fig. 1B), migration (Fig. 1C), and tube formation on Matrigel (Fig. 1D) were found to be significantly increased in *Ptprz1*$^{-/-}$ compared to *Ptprz1*$^{+/+}$ LMVEC. Basal phosphorylation levels of Akt at Ser 473 are also increased in *Ptprz1*$^{-/-}$ LMVEC, while ERK1/2 phosphorylation is not different between *Ptprz1*$^{-/-}$ and *Ptprz1*$^{+/+}$ LMVEC (Fig. 1E). Significantly enhanced angiogenesis was also observed in *Ptprz1*$^{-/-}$ compared to the *Ptprz1*$^{+/+}$ lungs *in vivo* (Fig. 1F). In the same line, radial sprouting of the vascular plexus is significantly higher in *Ptprz1*$^{-/-}$ compared to *Ptprz1*$^{+/+}$ retinas (Fig. S1); there is no significant difference in the endothelial tip cell density.

3.2 PTPRZ1 deletion enhances lung carcinogenesis and angiogenesis *in vivo*

Urethane was administered following the experimental timeline shown in Fig. 2A. Mice were sacrificed at week 24 unless they died earlier. The first interesting observation was that urethane-treated *Ptprz1*$^{-/-}$ mice had a significantly decreased survival compared to the *Ptprz1*$^{+/+}$ mice (Fig. 2B). In line with the decreased survival, the number of tumors per lung (Fig. 2C-D), tumor diameter and volume (Fig. 2E), as well as tumor burden per lung (Fig. 2F), were found significantly increased in the *Ptprz1*$^{-/-}$ compared to the *Ptprz1*$^{+/+}$ mice. Histological evaluation in H&E-stained paraffin-embedded lungs showed the presence of non-invasive, low-grade, yet fully developed adenocarcinomas in both groups. Nuclei were normal with mild to moderate atypia in some cells (Fig. 2G). *Ptprz1*$^{-/-}$ tumors have an increased number of PCNA-positive proliferating cells (Fig. 2H), increased angiogenesis (Fig. 2I), and significantly more macrophages compared to the *Ptprz1*$^{+/+}$ tumors (Fig. S2). No difference in the number of macrophages between *Ptprz1*$^{-/-}$ and *Ptprz1*$^{+/+}$ normal lungs was observed (Fig. S2). In the same mouse model of lung carcinogenesis [18, 22], PTPRZ1 expression is decreased in LUAD cells compared to adjacent normal lungs (Fig. S3A) or compared to lungs of saline- and urethane-treated mice obtained at one-week post-treatment, or to primary mouse tracheal epithelial cells (Fig S3B). PTPRZ1 expression

in urethane-treated *Ptprz1*$^{+/+}$ lungs is observed in bronchial epithelial cells and cancer cells (Fig. 2J).

3.3 Transcriptomic analysis of *Ptprz1*$^{+/+}$ and *Ptprz1*$^{-/-}$ LMVEC

To identify genes that may be involved in the enhanced angiogenic activities of *Ptprz1*$^{-/-}$ LMVEC, RNA sequencing analysis was performed, using total RNA isolated from *Ptprz1*$^{-/-}$ and *Ptprz1*$^{+/+}$ LMVEC. A pairwise comparison of gene expression of *Ptprz1*$^{-/-}$ RNA against *Ptprz1*$^{+/+}$ RNA identified several transcripts as differentially expressed in the Venn diagram (Fig. S4A and Table S2). Twenty-six genes were significantly changed (adjusted P value <0.05), with 9 being upregulated and 17 downregulated, as shown by the Volcano plot in Fig. S4B and the heat map of cluster analysis in Fig. S4C. The fold changes and the identity of these 26 genes are shown in Fig. S4D. Gene Ontology (GO) enrichment analysis categorized seven of the differentially expressed genes (*Tbx2, Tbx20, Hand2, Pitx2, Ctsh, Hpgd,* and *Thsd7a*) as linked to angiogenesis and tube formation (Fig. S4E). The *Ptprz1* gene does not show up in Fig. S4D, possibly because the strategy used to generate this knockout was to replace one exon in the opposite direction to *Ptprz1* gene transcription [13]. PTPRZ1 is not expressed in *Ptprz1*$^{-/-}$ mice [13], lungs (Fig. 2J and Fig. S5), or LMVEC (Fig. 1A), verified by our routine genotyping of the inbred mice. Besides these 26 genes, several more genes may be significantly affected by PTPRZ1 deletion, having P<0.01 although the adjusted P values are not <0.05 (Table S2). We focused on *itgb3* which encodes β_3 integrin and has a log2 fold change value of −0.847 in *Ptprz1*$^{-/-}$ compared to *Ptprz1*$^{+/+}$ LMVEC, P=0.008, and adjusted P=0.91. We found that the protein levels of β_3 integrin are significantly decreased in *Ptprz1*$^{-/-}$ compared to *Ptprz1*$^{+/+}$ LMVEC (Fig. 3A). To test whether the decreased β_3 integrin expression in *Ptprz1*$^{-/-}$ LMVEC may be linked to their enhanced angiogenic properties, we down-regulated β_3 integrin expression by siRNA (Fig. 3B) and found that it results in a significant enhancement of LMVEC growth (Fig. 3C) and migration (Fig. 3D). In agreement, β_3 overexpression in LMVEC significantly inhibits their migration, with a mild but statistically significant inhibitory effect on their proliferation (Fig. S6).

3.4 VEGFR2 and c-Met are activated in *Ptprz1*$^{-/-}$ LMVEC but only c-Met inhibition abolishes their enhanced angiogenic activities

Previous studies have shown that endothelial cells from β_3 integrin knockout mice have increased expression of VEGFR2, which is responsible for the observed enhanced angiogenesis following stimulation by $VEGFA_{165}$ [23]. Although our RNAseq data did not show alterations in VEGFR2 mRNA levels (Table S2), we found that VEGFR2 protein levels are increased in *Ptprz1*$^{-/-}$ compared to *Ptprz1*$^{+/+}$ LMVEC (Fig. S7A). VEGFA protein levels are also increased (Fig. S7B), resulting in a significantly enhanced VEGFR2 tyrosine phosphorylation in *Ptprz1*$^{-/-}$ compared to *Ptprz1*$^{+/+}$ LMVEC (Fig. S7C). The specific VEGFR2 inhibitor SU1498 abolished VEGFR2 tyrosine phosphorylation (Fig. S7C) and decreased both the proliferation and migration of *Ptprz1*$^{-/-}$ and *Ptprz1*$^{+/+}$ LMVEC. It did not, however, abolish the difference in the proliferation and migration potential of *Ptprz1*$^{-/-}$ compared to *Ptprz1*$^{+/+}$ LMVEC (Fig. S7D and E), suggesting that VEGFR2 is not indispensable for the enhanced angiogenic properties of *Ptprz1*$^{-/-}$ compared to *Ptprz1*$^{+/+}$ LMVEC.

It was recently shown that β_3 loss in mural cells leads to c-Met activation [24]. We, therefore, looked for c-Met activation in *Ptprz1*$^{-/-}$ LMVEC and found that c-Met tyrosine phosphorylation, but not c-Met mRNA or protein levels, is significantly enhanced in *Ptprz1*$^{-/-}$ compared to *Ptprz1*$^{+/+}$ LMVEC (Table S2 and Fig. 3E and F) and the difference is abolished by crizotinib (Fig. 3F), a small molecule c-Met TKI [29]. SU1498 does not affect c-Met tyrosine phosphorylation (Fig. S8A) and crizotinib does not affect VEGFR2 tyrosine phosphorylation in either *Ptprz1*$^{-/-}$ or *Ptprz1*$^{+/+}$ LMVEC (Fig. S8B). Crizotinib also inhibits Akt activation (Fig. 3G), proliferation (Fig. 3H), migration (Fig. 3I), and tube formation on Matrigel (Fig. 3J) in *Ptprz1*$^{-/-}$ LMVEC, while it does not affect *Ptprz1*$^{+/+}$ LMVEC. The enhanced c-Met activation observed in *Ptprz1*$^{-/-}$ LMVEC seems to be related to the decreased expression of β_3 integrin since the downregulation of β_3 in *Ptprz1*$^{+/+}$ LMVEC increased tyrosine phosphorylated c-Met levels (Fig. S9).

3.5 Crizotinib abolishes the enhanced lung carcinogenesis and angiogenesis observed in *Ptprz1*$^{-/-}$ mice

In the urethane model of lung carcinogenesis, starting at week 3 after the first injection of urethane, mice were weekly injected i.p. with 25 mg/kg crizotinib or the solvent control, for 11 weeks. Based on the decreased survival of the urethane-treated *Ptprz1*$^{-/-}$ mice described above, in this set of experiments, we sacrificed the animals at week 19 (Fig. 4A). However, survival of the *Ptprz1*$^{-/-}$ group was still impaired at 15 weeks after the first urethane injection, an effect that was not observed in the group that received crizotinib (Fig. 4B). The weight of the animals during the experiment was not affected (Fig. S10). Crizotinib significantly decreased the number of tumors per lung (Fig. 4C and D), tumor diameter and volume (Fig. 4E), and total tumor burden per lung (Fig. 4F) in *Ptprz1*$^{-/-}$ mice, with no effect in *Ptprz1*$^{+/+}$ mice. It also significantly inhibited the increased number of PCNA-positive proliferating cells in *Ptprz1*$^{-/-}$ tumors (Fig. 4G). No significant histological differences were observed between *Ptprz1*$^{-/-}$ and *Ptprz1*$^{+/+}$ tumors, in the presence or absence of crizotinib (Fig. 4H). Akt phosphorylation at Ser 473 (Fig. 4I) and c-Met tyrosine phosphorylation (Fig. 4J) were found to be significantly increased in *Ptprz1*$^{-/-}$ compared to *Ptprz1*$^{+/+}$ tumors and the difference was abolished by crizotinib. The latter also abolished the enhanced angiogenesis observed in *Ptprz1*$^{-/-}$ compared to *Ptprz1*$^{+/+}$ tumors (Fig. 4K), without affecting the preformed vessels in the adjacent normal lungs (Fig. S11). It also abolished the enhanced macrophage recruitment in *Ptprz1*$^{-/-}$ tumors (Fig. S12).

3.6 Inhibition of PTPRZ1 TP activity enhances *in vitro* angiogenesis through c-Met tyrosine phosphorylation

To investigate whether the TP activity of PTPRZ1 was responsible for the regulation of the angiogenic activities of endothelial cells, we used the selective PTPRZ1 TP inhibitor MY10 and found that it increases *Ptprz1*$^{+/+}$ LMVEC proliferation (Fig. 5A), migration (Fig. 5B), and tube formation on Matrigel (Fig. 5C), while it does not affect *Ptprz1*$^{-/-}$ LMVEC, suggesting that the pharmacological inhibition of the PTPRZ1 TP activity mimics PTPRZ1 deletion. Crizotinib abolishes the stimulatory effect of MY10 on *Ptprz1*$^{+/+}$ LMVEC proliferation (Fig. 5D), migration (Fig. 5E), tube formation on Matrigel (Fig. 5F), and c-Met tyrosine phosphorylation (Fig. 5G). Like its effect on *Ptprz1*$^{+/+}$ LMVEC, MY10 stimulates migration (Fig. S13A), as well as c-Met and Akt activation (Fig. S13B and C) in HUVEC,

all inhibited by crizotinib. Crizotinib also abolished the enhanced proliferation and migration observed in MY-10-treated LUAD cells isolated from the lungs of urethane-treated mice (Fig. S14).

3.7 $VEGFA_{165}$ and PTN activate c-Met in endothelial cells

Based on the above and our previous data showing that VEGFA binds to and requires PTPRZ1 to stimulate human endothelial cell migration [10], we tested whether $VEGFA_{165}$ activates c-Met. As shown in Fig 6A, $VEGFA_{165}$ significantly increases tyrosine phosphorylation of c-Met in HUVEC and crizotinib abolishes $VEGFA_{165}$-induced HUVEC proliferation (Fig. 6B), migration (Fig. 6C), and Akt activation (Fig. 6D), suggesting that c-Met activation is required for VEGFA signaling independently of VEGFR2. In support of this, SU1498 does not affect $VEGFA_{165}$-induced Akt activation (Fig. S15A) and crizotinib does not affect $VEGFA_{165}$-induced VEGFR2 tyrosine phosphorylation or ERK1/2 activation (Fig. S15B and C). PTN, which competes with VEGFA for binding to PTPRZ1 [10], also enhances c-Met tyrosine phosphorylation (Fig. 6E) and crizotinib abolishes PTN-induced HUVEC migration (Fig. 6F). Involvement of PTPRZ1 in VEGFA- and PTN-induced c-Met activation is also supported by the observation that both $VEGFA_{165}$ and PTN stimulate migration of *Ptprz1*$^{+/+}$ LMVEC but have no effect on the already enhanced *Ptprz1*$^{-/-}$ LMVEC migration (Fig. 6G). Similarly, in HUVEC, MY10 stimulates cell migration and in MY10-stimulated HUVEC, PTN or $VEGFA_{165}$ have no effect (Fig. 6H).

4. Discussion

In the present work, in an animal model that mimics LUAD development in smokers, we show that the decreased PTPRZ1 expression favors LUAD growth and angiogenesis suggesting that PTPRZ1 expression may be added to the biomarkers for LUAD prognosis. This is further supported by our observation that decreased PTPRZ1 expression leads to decreased animal survival, in line with TCGA data showing that the decreased PTPRZ1 gene expression is inversely correlated to patient overall survival [8]. Our IHC data, as well as data from the Human Protein Atlas, show that PTPRZ1 gene expression in the adult lung is mostly restricted to the club and respiratory cells (Single cell type - PTPRZ1 - The Human Protein Atlas), which are important for chemically induced LUAD development [18]; our data suggest that the decreased PTPRZ1 expression enhances club cell transformation to LUAD cells. The presence of a *Ptprz1* gene inactivating mutation or epigenetic silencing might also be indicative of a worse LUAD prognosis and should be considered. Such epigenetic event has been observed in colorectal tumors, where the *Ptprz1* promoter is hypermethylated compared to matched normal tissue, without any association between the methylation status and other driver mutations or tumor localization [26].

Besides increased tumor growth, PTPRZ1 deletion leads to increased angiogenesis *in vivo* and enhanced endothelial cells' proliferation, migration, and tube formation *in vitro*, through down-regulation of β_3 integrin expression and activation of tyrosine kinase receptors. The notion of enhanced angiogenesis and carcinogenesis due to decreased β_3 integrin expression is in line with several previous data showing an inhibitory role of β_3 integrin in glioblastoma cell migration [27], osteopontin-induced non-small cell lung cancer cell growth [28], and

VEGFA-induced endothelial cell proliferation and migration [23]. It is also in line with the enhanced tumor growth and angiogenesis observed in *itgb3*$^{-/-}$ mice [29] and the enhanced c-Met-dependent tumor growth observed when expression of β_3 is deleted in mural cells [24]. One point that needs to be clarified by future studies is what happens when PTPRZ1 is not deleted but its TP activity is inhibited, as is the case with MY10, PTN, and $VEGFA_{165}$. We have previously shown in endothelial cells that PTN and $VEGFA_{165}$ induce β_3 Tyr773 phosphorylation and PTPRZ1 is required for this effect [10, 30]. To date, it is not known whether this phosphorylation affects β_3 stability. Under membrane-mimetic conditions, it has been shown that β_3 tyrosine phosphorylation perturbs its overall fold and modifies its membrane embedding [31], which might mimic decreased β_3 integrin expression. Further studies are underway to elucidate this point.

The observation that PTN and $VEGFA_{165}$ stimulate migration of *Ptprz1*$^{+/+}$ LMVEC but do not affect the already enhanced *Ptprz1*$^{-/-}$ LMVEC migration, suggests that the pathway activated by $VEGFA_{165}$ and PTN in *Ptprz1*$^{+/+}$ LMVEC is already activated in *Ptprz1*$^{-/-}$ LMVEC. In the same line, neither PTN nor $VEGFA_{165}$ affects the migration of HUVEC in the presence of the PTPRZ1 TP inhibitor, supporting the notion that the enhanced cell migration caused by PTN or $VEGFA_{165}$ is due to the inhibition of PTPRZ1 TP activity. This has been previously described for PTN [1, 8] but not for VEGFA. Downstream of PTPRZ1 TP inactivation, $VEGFA_{165}$ activates Akt, in line with previous data in ovarian cancer cells showing that PTPRZ1 negatively regulates Akt kinase activity [6]. The $VEGFA_{165}$-induced Akt activation is not dependent on VEGFR2 TK activity but is abolished by the c-Met TKI crizotinib, highlighting the significance of the interplay between PTPRZ1 and c-Met for VEGFA signaling. Crizotinib does not affect phosphorylation and thus activation of VEGFR2 or ERK1/2, suggesting that its effects on c-Met and Akt activation are selective and that c-Met activation is required for VEGFA signaling and activities. On the other hand, it is well known that inhibition of VEGFA binding to VEGFR2 inhibits VEGFA-induced endothelial cell activation [12]. It seems, therefore, that binding of VEGFA to VEGFR2 and PTPRZ1 activates VEGFR2 and c-Met, respectively, to activate endothelial cells. It is of interest to study whether PTPRZ1 may mediate the effects of VEGFA in cancer cells that do not express VEGFR2 and whether such a pathway may significantly affect cancer cell growth and/or angiogenesis.

Besides mediating the stimulatory effects of $VEGFA_{165}$ and PTN on endothelial cell migration, cMet seems to also mediate LUAD growth and angiogenesis *in vivo*, but only when PTPRZ1 expression is downregulated. This is supported by the observation that c-Met seems to be activated only in *Ptprz1*$^{-/-}$ tumors and is inhibited in mice treated with crizotinib, in line with the effect of crizotinib in LUAD growth and angiogenesis. In the same line, cMet seems to mediate the enhanced proliferation and migration of the LUAD cells *in vitro* observed when the PTPRZ1 TP activity is inhibited. Ligand-independent c-Met activation has been shown in a subset of LUAD patients and in that immunohistochemical analysis, phosphorylated c-Met was correlated to phosphorylated Akt but not ERK1/2 [32], in line with our data showing that phosphorylated Akt but not ERK1/2 is increased in *Ptprz1*$^{-/-}$ LMVEC and LUAD. Our data propose the use of crizotinib or other c-Met TKIs in LUAD patients with decreased PTPRZ1 expression, independently of other driver mutations, favoring the exploitation of PTPRZ1 gene expression as a potential predictive biomarker

for LUAD response to such drugs. It should be noted that although inhibition of c-Met by crizotinib inhibits LUAD angiogenesis, it does not affect the vessels that were formed before crizotinib administration in the *Ptprz1*$^{-/-}$ normal lungs, suggesting that c-Met inhibition decreases new vessel formation but does not harm pre-formed vessels.

The fully developed adenocarcinomas in both *Ptprz1*$^{-/-}$ and *Ptprz1*$^{+/+}$ lungs showed no histological differences, but cell proliferation and macrophage recruitment were significantly higher in *Ptprz1*$^{-/-}$ compared to *Ptprz1*$^{+/+}$ LUAD. Proliferation is a well-described activity downstream of c-Met activation [33], and the number of actively proliferating cells in *Ptprz1*$^{-/-}$ LUAD is decreased upon crizotinib administration, in line with the effect of crizotinib on tumor number, size, and burden. Macrophages are significant for the progression of urethane-induced LUAD in mice [34] and the increased number of macrophages observed in the *Ptprz1*$^{-/-}$ tumors agrees with the increased tumor burden and angiogenesis. The inhibitory effect of crizotinib suggests that the enhanced c-Met TK activity may have a role in this recruitment, adding to the previously published observation that c-Met activation contributes to shifting the M1 toward the pro-tumorigenic M2 macrophage phenotype [35].

Collectively, our data suggest that PTPRZ1 deficiency results in decreased β_3 integrin protein levels and activation of c-Met and Akt, leading to endothelial cell stimulation, angiogenesis enhancement, and LUAD growth. VEGFA, PTN, and a selective PTPRZ1 TP inhibitor, also activate c-Met and Akt in a PTPRZ1-dependent manner in endothelial cells. The c-Met TKI crizotinib abolishes the stimulatory effects of PTPRZ1 deficiency *in vitro* and *in vivo* and of PTPRZ1 TP inhibition *in vitro* (Fig. 6I), supporting a potential therapeutic benefit of c-Met TKIs for LUAD patients with low PTPRZ1 expression. Since VEGFA binds to PTPRZ1 in a VEGFR2-independent manner [10, 11], our data also warrant further investigation of the potential targeting of PTPRZ1 as an alternative therapeutic approach in anti-VEGFA/VEGFR2-resistant angiogenesis.

Supplementary Material

Refer to Web version on PubMed Central for supplementary material.

Acknowledgments

The authors are grateful to Dr. Heather Himburg and Prof. John Chute at the Division of Haematology/Oncology, Broad Stem Cell Research Centre, UCLA, Los Angeles, USA, for kindly providing the *Ptprz1*$^{-/-}$ and *Ptprz*$^{+/+}$ mice, and Drs Maria Hatziapostolou and Christos Polytarchou at the Department of Biosciences, John van Geest Cancer Research Centre, School of Science and Technology, Nottingham Trent University, Nottingham, United Kingdom, for transferring them. They also wish to thank Dr. Margarita Lamprou for her technical support on the pVEGFR2 Western blots and the Advanced Light Microscopy facilities of the School of Health Sciences and the Department of Biology, University of Patras, for using the Leica SP5 confocal microscopes.

Funding

This work has been financed by the State Scholarship Foundation in Greece (IKY) (Operational Program “Human Resources Development – Education and Lifelong Learning”, Partnership Agreement 2014-2020, scholarships to PK, DNt, EM, and EC), a University of Patras “Andreas Mentzelopoulos” scholarship (to M-KE), an FP7 People: Marie Curie Intra European Fellowship (#626057) and Matching Funds (to EvP), and an FP7 Ideas: European Research Council 2010 Starting Independent Investigator (#260524) and 2015 Proof of Concept (#679345) grants (to GTS). The work performed at Texas Tech University Health Sciences Center (TTUHSC) was supported in part by the National Institutes of Health Grant (NCI) R15CA231339 and the TTUHSC School of Pharmacy Office

of the Sciences grant. The common equipment used at TTUHSC was obtained through the Cancer Prevention Research Institute of Texas (CPRIT) Grants RP110786, RP190524, and RP200572. The funders had no role in the study design, decision to write, or preparation of the manuscript.

Data availability

The raw reads of transcriptomic data are deposited in the Gene Expression Omnibus (GEO, accession number: GSE161080) at the National Centre for Biotechnology Information (NCBI). Other data that support the findings of this study are available from the corresponding author upon request.

List of abbreviations:

LMVEC	lung microvascular endothelial cells
LUAD	lung adenocarcinoma
PTN	pleiotrophin
PTPRZ1	protein tyrosine phosphatase receptor zeta 1
TK	tyrosine kinase
TKI	tyrosine kinase inhibitor
TP	tyrosine phosphatase
VEGFA	vascular endothelial growth factor A
VEGFR2	vascular endothelial growth factor receptor 2

References

1. Papadimitriou E, Pantazaka E, Castana P, Tsalios T, Polyzos A, Beis D. Pleiotrophin and its receptor protein tyrosine phosphatase beta/zeta as regulators of angiogenesis and cancer. Biochim Biophys Acta 2016; 1866: 252–265. [PubMed: 27693125]
2. Fujikawa A, Sugawara H, Tanaka T, Matsumoto M, Kuboyama K, Suzuki R, et al. Targeting PTPRZ inhibits stem cell-like properties and tumorigenicity in glioblastoma cells. Sci Rep 2017; 7: 5609. [PubMed: 28717188]
3. Yoon SJ, Baek S, Yu SE, Jo E, Lee D, Shim JK, Choi RJ, Park J, Moon JH, Kim EH, Chang JH, Lee JB, Park JS, Sung HJ, Kang SG. Tissue Niche Miniature of Glioblastoma Patient Treated with Nano-Awakeners to Induce Suicide of Cancer Stem Cells. Adv Healthc Mater 2022; 11: e2201586. [PubMed: 36047642]
4. Makinoshima H, Ishii G, Kojima M, Fujii S, Higuchi Y, Kuwata T, Ochiai A. PTPRZ1 regulates calmodulin phosphorylation and tumor progression in small-cell lung carcinoma. BMC Cancer 2012; 12: 537. [PubMed: 23170925]
5. Diamantopoulou Z, Kitsou P, Menashi S, Courty J, Katsoris P. Loss of receptor protein tyrosine phosphatase β/ζ (RPTPβ/ζ) promotes prostate cancer metastasis. J Biol Chem 2012; 287: 40339–10349. [PubMed: 23060448]
6. Baldauf C, Jeschke A, Kanbach V, Catala-Lehnen P, Baumhoer D, Gerull H, Buhs S, Amling M, Nollau P, Harroch S, Schinke T. The Protein Tyrosine Phosphatase Rptpζ Suppresses Osteosarcoma Development in Trp53-Heterozygous Mice. PLoS One 2015; 10: e0137745. [PubMed: 26360410]

7. Wang P, Hu Y, Qu P, Zhao Y, Liu J, Zhao J, Kong B. Protein tyrosine phosphatase receptor type Z1 inhibits the cisplatin resistance of ovarian cancer by regulating PI3K/AKT/mTOR signal pathway. Bioengineered 2022; 13: 1931–1341. [PubMed: 35001804]

8. Xia Z, Ouyang D, Li Q, Li M, Zou Q, Li L, Yi W, Zhou E. The Expression, Functions, Interactions and Prognostic Values of PTPRZ1: A Review and Bioinformatic Analysis. J Cancer 2019; 10:663–74.

9. Polykratis A, Katsoris P, Courty J, Papadimitriou E. Characterization of heparin affin regulatory peptide signaling in human endothelial cells. J Biol Chem 2005; 280: 22454–22461. [PubMed: 15797857]

10. Koutsioumpa M, Poimenidi E, Pantazaka E, Theodoropoulou C, Skoura A, Megalooikonomou V, Kieffer N, Courty J, Mizumoto S, Sugahara K, Papadimitriou E. Receptor protein tyrosine phosphatase beta/zeta is a functional binding partner for vascular endothelial growth factor. Mol Cancer 2015; 14: 19. [PubMed: 25644401]

11. Poimenidi E, Theodoropoulou C, Koutsioumpa M, Skondra L, Droggiti E, van den Broek M, Koolwijk P, Papadimitriou E. Vascular endothelial growth factor A (VEGF-A) decreases expression and secretion of pleiotrophin in a VEGF receptor-independent manner. Vascul Pharmacol 2016; 80: 11–19. [PubMed: 26924457]

12. Eelen G, Treps L, Li X, Carmeliet P. Basic and Therapeutic Aspects of Angiogenesis Updated. Circ Res 2020; 127: 310–329. [PubMed: 32833569]

13. Harroch S, Palmeri M, Rosenbluth J, Custer A, Okigaki M, Shrager P, Blum M, Buxbaum JD, Schlessinger J. No obvious abnormality in mice deficient in receptor protein tyrosine phosphatase beta. Mol Cell Biol 2000; 20: 7706–7715. [PubMed: 11003666]

14. Zahra FT, Sajib MS, Ichiyama Y, Akwii RG, Tullar PE, Cobos C, Minchew SA, Doçi CL, Zheng Y, Kubota Y, Gutkind JS, Mikelis CM. Endothelial RhoA GTPase is essential for in vitro endothelial functions but dispensable for physiological in vivo angiogenesis. Sci Rep 2019; 9: 11666. [PubMed: 31406143]

15. Agalioti T, Giannou AD, Krontira AC, Kanellakis NI, Kati D, Vreka M, Pepe M, Spella M, Lilis I, Zazara DE, Nikolouli E, Spiropoulou N, Papadakis A, Papadia K, Voulgaridis A, Harokopos V, Stamou P, Meiners S, Eickelberg O, Snyder LA, Antimisiaris SG, Kardamakis D, Psallidas I, Marazioti A, Stathopoulos GT. Mutant KRAS promotes malignant pleural effusion formation. Nat Commun 2017; 8: 15205. [PubMed: 28508873]

16. Kanellakis NI, Giannou AD, Pepe MAA, Agalioti T, Zazara DE, Giopanou I, Psallidas I, Spella M, Marazioti A, Arendt KAM, Lamort AS, Champeris Tsaniras S, Taraviras S, Papadaki H, Lilis I, Stathopoulos GT. Tobacco chemical-induced mouse lung adenocarcinoma cell lines pin the prolactin orthologue proliferin as a lung tumour promoter. Carcinogenesis 2019; 40: 1352–1362. [PubMed: 30828726]

17. Pastor M, Fernández-Calle R, Di Geronimo B, Vicente-Rodríguez M, Zapico JM, Gramage E, Coderch C, Pérez-García C, Lasek AW, Puchades-Carrasco L, Pineda-Lucena A, de Pascual-Teresa B, Herradón G, Ramos A. Development of inhibitors of receptor protein tyrosine phosphatase β/ζ (PTPRZ1) as candidates for CNS disorders. Eur J Med Chem 2018; 144: 318–329. [PubMed: 29275231]

18. Spella M, Lilis I, Pepe MA, Chen Y, Armaka M, Lamort AS, Zazara DE, Roumelioti F, Vreka M, Kanellakis NI, Wagner DE, Giannou AD, Armenis V, Arendt KA, Klotz LV, Toumpanakis D, Karavana V, Zakynthinos SG, Giopanou I, Marazioti A, Aidinis V, Sotillo R, Stathopoulos GT. Club cells form lung adenocarcinomas and maintain the alveoli of adult mice. Elife 2019; 8: e45571. [PubMed: 31140976]

19. Stathopoulos GT, Sherrill TP, Cheng DS, Scoggins RM, Han W, Polosukhin VV, Connelly L, Yull FE, Fingleton B, Blackwell TS. Epithelial NF-kappaB activation promotes urethane-induced lung carcinogenesis. Proc Natl Acad Sci USA 2007; 104: 18514–18519. [PubMed: 18000061]

20. Jackson EL, Olive KP, Tuveson DA, Bronson R, Crowley D, Brown M, Jacks T. The differential effects of mutant p53 alleles on advanced murine lung cancer. Cancer Res 2005; 65: 10280–10288. [PubMed: 16288016]

21. Katraki-Pavlou S, Kastana P, Bousis D, Ntenekou D, Varela A, Davos CH, Nikou S, Papadaki E, Tsigkas G, Athanasiadis E, Herradon G, Mikelis CM, Beis D, Papadimitriou E. Protein tyrosine

phosphatase receptor-ζ1 deletion triggers defective heart morphogenesis in mice and zebrafish. Am J Physiol Heart Circ Physiol 2022; 322: H8–H24. [PubMed: 34767486]

22. Stearman RS, Dwyer-Nield L, Zerbe L, Blaine SA, Chan Z, Bunn PA Jr, Johnson GL, Hirsch FR, Merrick DT, Franklin WA, Baron AE, Keith RL, Nemenoff RA, Malkinson AM, Geraci MW. Analysis of orthologous gene expression between human pulmonary adenocarcinoma and a carcinogen-induced murine model. Am J Pathol 2005; 167: 1763–1775. [PubMed: 16314486]
23. Reynolds AR, Reynolds LE, Nagel TE, Lively JC, Robinson SD, Hicklin DJ, Bodary SC, Hodivala-Dilke KM. Elevated Flk1 (vascular endothelial growth factor receptor 2) signaling mediates enhanced angiogenesis in beta3-integrin-deficient mice. Cancer Res 2004; 64: 8643–8650. [PubMed: 15574772]
24. Wong PP, Muñoz-Félix JM, Hijazi M, Kim H, Robinson SD, De Luxán-Delgado B, Rodríguez-Hernández I, Maiques O, Meng YM, Meng Q, Bodrug N, Dukinfield MS, Reynolds LE, Elia G, Clear A, Harwood C, Wang Y, Campbell JJ, Singh R, Zhang P, Schall TJ, Matchett KP, Henderson NC, Szlosarek PW, Dreger SA, Smith S, Jones JL, Gribben JG, Cutillas PR, Meier P, Sanz-Moreno V, Hodivala-Dilke KM. Cancer Burden Is Controlled by Mural Cell-β3-Integrin Regulated Crosstalk with Tumor Cells. Cell 2020; 181: 1346–1363.e21. [PubMed: 32473126]
25. Puccini A, Marín-Ramos NI, Bergamo F, Schirripa M, Lonardi S, Lenz HJ, Loupakis F, Battaglin F. Safety and Tolerability of c-MET Inhibitors in Cancer. Drug Saf 2019; 42: 211–233. [PubMed: 30649748]
26. Laczmanska I, Karpinski P, Bebenek M, Sedziak T, Ramsey D, Szmida E, Sasiadek MM. Protein tyrosine phosphatase receptor-like genes are frequently hypermethylated in sporadic colorectal cancer. J Hum Genet 2013; 58: 11–15. [PubMed: 23096495]
27. Lamprou M, Kastana P, Kofina F, Tzoupis H, Barmpoutsi S, Sajib MS, Koutsioumpa M, Poimenidi E, Zompra AA, Tassopoulos D, Choleva E, Tselios T, Mikelis CM, Papadimitriou E. Pleiotrophin selectively binds to vascular endothelial growth factor receptor 2 and inhibits or stimulates cell migration depending on αvβ3 integrin expression. Angiogenesis 2020; 23: 621–636. [PubMed: 32681389]
28. Sun SJ, Wu CC, Sheu GT, Chang HY, Chen MY, Lin YY, Chuang CY, Hsu SL, Chang JT. Integrin β3 and CD44 levels determine the effects of the OPN-a splicing variant on lung cancer cell growth. Oncotarget 2016; 7: 55572–55784. [PubMed: 27487131]
29. Reynolds LE, Wyder L, Lively JC, Taverna D, Robinson SD, Huang X, Sheppard D, Hynes RO, Hodivala-Dilke KM. Enhanced pathological angiogenesis in mice lacking beta3 integrin or beta3 and beta5 integrins. Nat Med 2002; 8: 27–34. [PubMed: 11786903]
30. Mikelis C, Sfaelou E, Koutsioumpa M, Kieffer N, Papadimitriou E. Integrin alpha(v)beta(3) is a pleiotrophin receptor required for pleiotrophin-induced endothelial cell migration through receptor protein tyrosine phosphatase beta/zeta. FASEB J 2009; 23: 1459–1469. [PubMed: 19141530]
31. Deshmukh L, Meller N, Alder N, Byzova T, Vinogradova O. Tyrosine phosphorylation as a conformational switch: a case study of integrin β3 cytoplasmic tail. J Biol Chem 2011; 286: 40943–40953. [PubMed: 21956114]
32. Nakamura Y, Niki T, Goto A, Morikawa T, Miyazawa K, Nakajima J, Fukayama M. c-Met activation in lung adenocarcinoma tissues: an immunohistochemical analysis. Cancer Sci 2007; 98: 1006–1013. [PubMed: 17459054]
33. Friedlaender A, Drilon A, Banna GL, Peters S, Addeo A. The METeoric rise of MET in lung cancer. Cancer 2020; 126: 4826–4837. [PubMed: 32888330]
34. Zaynagetdinov R, Stathopoulos GT, Sherrill TP, Cheng DS, McLoed AG, Ausborn JA, Polosukhin VV, Connelly L, Zhou W, Fingleton B, Peebles RS, Prince LS, Yull FE, Blackwell TS. Epithelial nuclear factor-κB signaling promotes lung carcinogenesis via recruitment of regulatory T lymphocytes. Oncogene 2012; 31: 3164–3176. [PubMed: 22002309]
35. Nishikoba N, Kumagai K, Kanmura S, Nakamura Y, Ono M, Eguchi H, Kamibayashiyama T, Oda K, Mawatari S, Tanoue S, Hashimoto S, Tsubouchi H, Ido A. HGF-MET Signaling Shifts M1 Macrophages Toward an M2-Like Phenotype Through PI3K-Mediated Induction of Arginase-1 Expression. Front Immunol 2020; 11: 2135. [PubMed: 32983173]

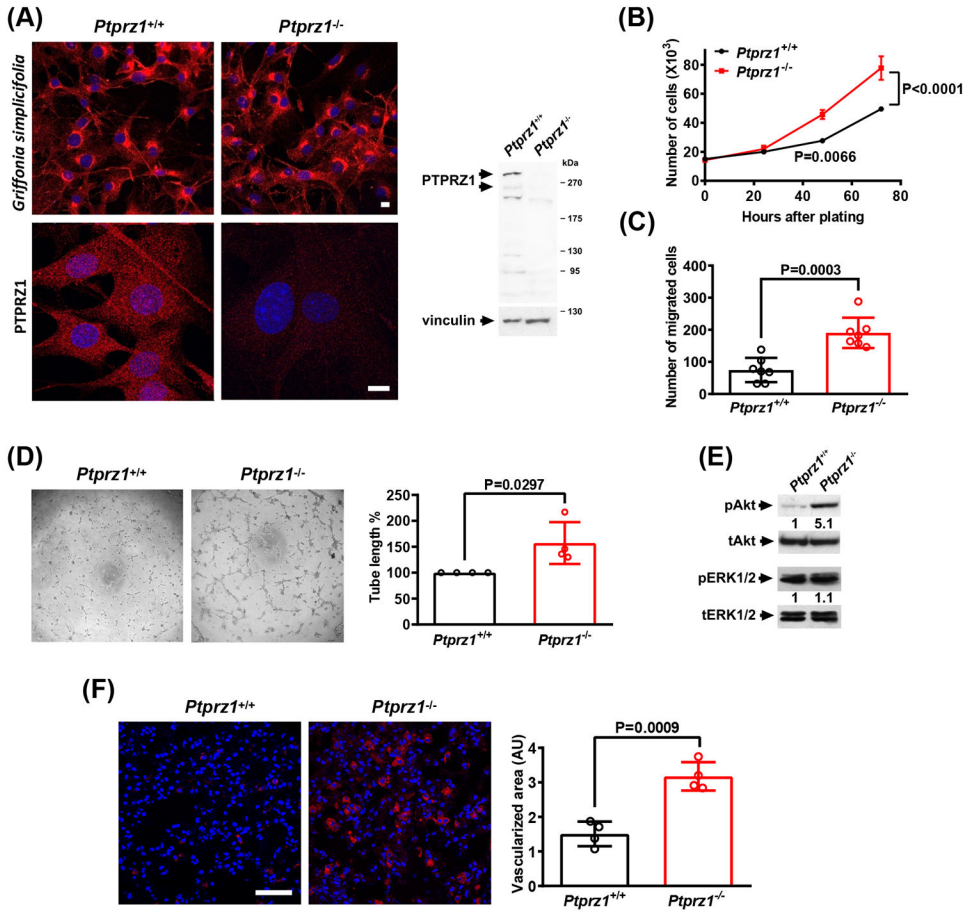

Fig. 1. PTPRZ1 deletion enhances LMVEC angiogenic activities *in vitro* and physiological lung angiogenesis *in vivo*.

(A) *Left:* LMVEC isolated from *Ptprz1*$^{+/+}$ and *Ptprz1*$^{-/-}$ mice stained with rhodamine-conjugated *Griffonia simplicifolia* lectin as a marker of mouse endothelial cells or with an antibody specific for PTPRZ1 (red). Nuclei are stained with Draq5 (blue), and scale bars correspond to 10 μm. *Right*: Western blot analysis for PTPRZ1 in total protein extracts of *Ptprz1*$^{+/+}$ and *Ptprz1*$^{-/-}$ LMVEC. Vinculin is used as a loading control. **(B)** Numbers of *Ptprz1*$^{-/-}$ and *Ptprz1*$^{+/+}$ LMVEC at different time points after plating (mean ± SD, n=6). **(C)** Migration of *Ptprz1*$^{-/-}$ and *Ptprz1*$^{+/+}$ LMVEC using the transwell assay (mean ± SD). **(D)** Representative photos and quantification of the tube network formed by *Ptprz1*$^{-/-}$ and *Ptprz1*$^{+/+}$ LMVEC on Matrigel. Results are expressed as mean ± SD of the percent tube length compared to the *Ptprz1*$^{+/+}$ cells (set as default 100%). **(E)** LMVEC whole cell lysates were analyzed by antibodies against Akt phosphorylated at Ser473 (pAkt), total Akt (tAkt), ERK1/2 phosphorylated at Tyr895 (pERK1/2), and total ERK1/2 (tERK1/2). Representative Western blots are shown (n=3). Numbers denote the average fold change of the ratio pAkt/tAkt or pERK1/2/tERK1/2 compared to *Ptprz1*$^{+/+}$ LMVEC (set as default = 1). **(F)** Paraffin-embedded normal lung *Ptprz1*$^{-/-}$ and *Ptprz1*$^{+/+}$ tissue sections stained with rhodamine-conjugated *Griffonia simplicifolia* lectin for endothelial cells (red). Nuclei are stained with Draq5 (blue). Representative pictures are shown, and the scale bar corresponds

to 50 μm. Results are expressed as mean ± SD of the vascularized area per field of lung tissue in arbitrary units (AU).

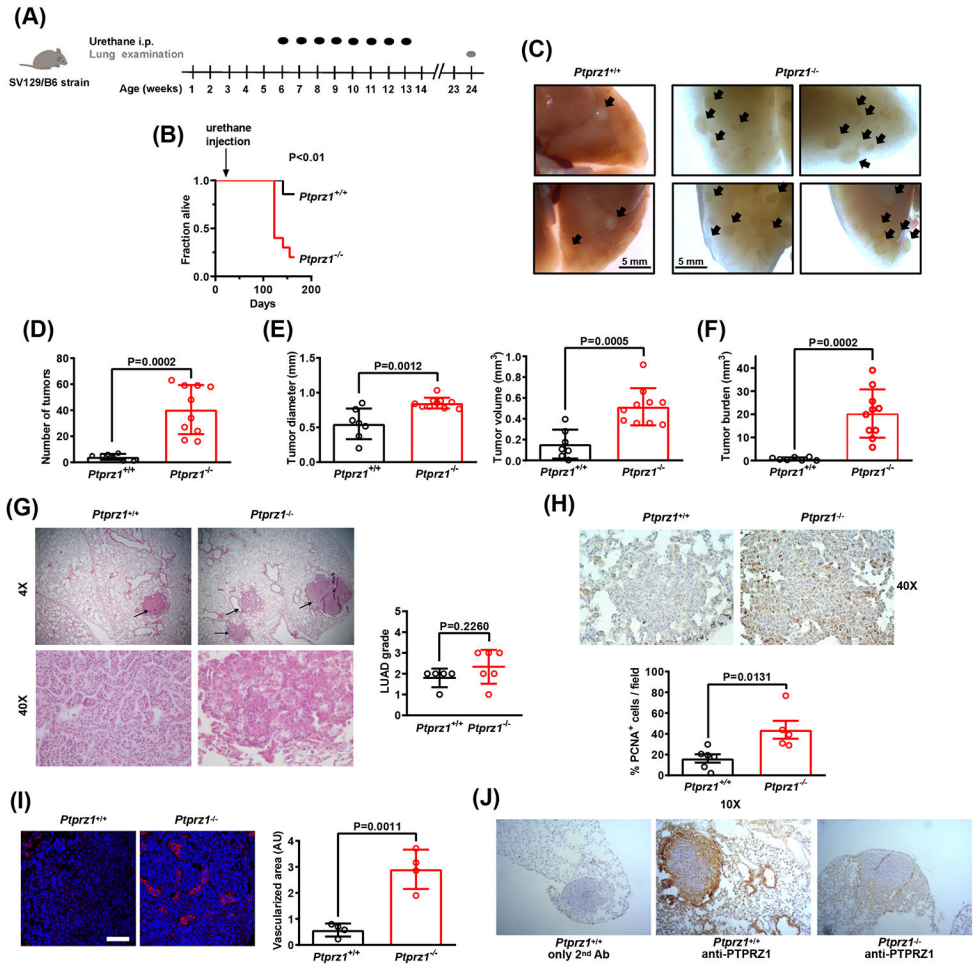

Fig. 2. PTPRZ1 deletion enhances lung carcinogenesis and angiogenesis *in vivo*.

(A) Schematic representation of the experimental timeline. **(B)** Kaplan-Meier plot of *Ptprz1*$^{-/-}$ and *Ptprz1*$^{+/+}$ mice survival. Statistical analysis was performed by using the Log-rank (Mantel-Cox) test. **(C)** Representative images of the lungs at the end of the experiment. Arrows indicate tumors. The number of tumors per lung **(D)**, tumor diameter and volume **(E)**, and total tumor burden per lung **(F)** are presented as mean ± SD. **(G)** Representative pictures from H&E-stained tumor tissue sections at 4x and 40x magnification. The arrows at 4x magnification point to tumors. Grading of urethane-induced tumors was estimated blindly on a scale from 1 to 5, with 1 indicating the lowest grade. **(H)** Representative pictures at 40x magnification of *Ptprz1*$^{-/-}$ and *Ptprz1*$^{+/+}$ tumor tissue sections stained for PCNA (brown) and counterstained by hematoxylin (blue). Results are expressed as mean ± SD of the percent number of PCNA stained (PCNA^{+}) cells per field of tumor tissue. **(I)** Paraffin-embedded *Ptprz1*$^{-/-}$ and *Ptprz1*$^{+/+}$ LUAD tissue sections stained for endothelial cells (red) and nuclei (blue). Representative pictures are shown, and the scale bar corresponds to 50 μm. Results are expressed as mean ± SD of the vascularized area per field of LUAD in arbitrary units (AU). **(J)** Representative pictures at 10x magnification of urethane-treated *Ptprz1*$^{-/-}$ and *Ptprz1*$^{+/+}$ lung tissue sections stained for PTPRZ1 (brown) and counterstained by hematoxylin (blue). *Ptprz1*$^{-/-}$ lungs were used as a negative control.

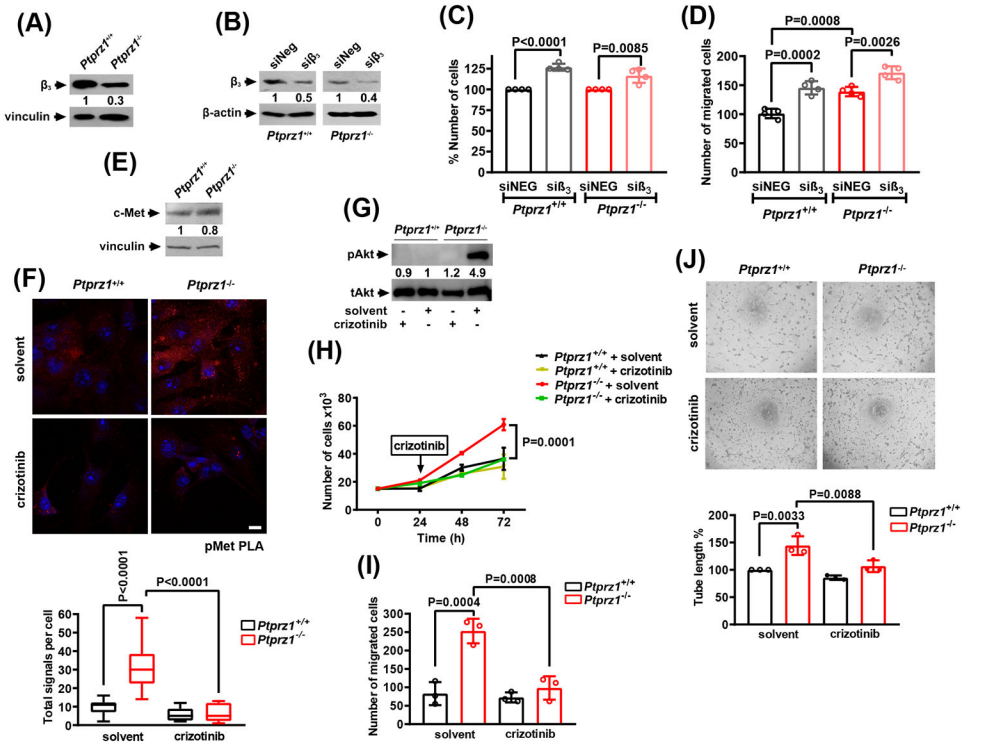

Fig. 3. Decreased β_3 integrin expression and c-Met activation enhance LMVEC proliferation and migration.

(A) LMVEC whole cell lysates were analyzed by antibodies against β_3 integrin and vinculin (used as a loading control). Representative Western blots are shown (n=3). Numbers denote the average fold change of the ratio β_3/vinculin compared to *Ptprz1*$^{+/+}$ LMVEC (set as default = 1). **(B)** LMVEC whole cell lysates following downregulation of β_3 by siRNA were analyzed using antibodies against β_3 integrin and β-actin. Representative Western blots are shown (n=3). Numbers denote the average fold change of the ratio β_3/β-actin compared to the corresponding siNeg-treated LMVEC (set as default = 1). **(C)** Cell proliferation following downregulation of β_3 integrin. Results are expressed as mean ± SD of the percent number of cells compared to the corresponding control (set as default 100%). **(D)** Cell migration following downregulation of β_3 integrin. Results are expressed as mean ± SD. siNeg, cells transfected with a negative control siRNA; siβ_3, cells transfected with siRNA for β_3. **(E)** LMVEC whole cell lysates were analyzed by antibodies against c-Met and vinculin (used as a loading control). Representative Western blots are shown (n=3). Numbers denote the average fold change of the ratio c-Met/vinculin compared to *Ptprz1*$^{+/+}$ LMVEC (set as default = 1). **(F)** Formation of pTyr-c-Met complexes as evidenced by in situ PLA. Cells were incubated with crizotinib (1 μM) or the corresponding solvent for 2 h and then fixed and stained for tyrosine phosphorylated c-Met (pMet). Representative pictures are shown. The scale bar corresponds to 10 μm. The box plots indicate the median, mean, and range of the detected signals (n = 8-10 image fields with 3-6 cells per image per sample type, each sample run in triplicate). **(G)** Whole cell lysates of *Ptprz1*$^{+/+}$ and *Ptprz1*$^{-/-}$ LMVEC cultured in the presence or absence of crizotinib were analyzed by antibodies against Akt phosphorylated at Ser473 (pAkt) and total Akt (tAkt). Representative Western blots are shown (n=3). Numbers denote the average fold change of the ratio pAkt/tAkt

compared to untreated *Ptprz1*$^{+/+}$ LMVEC (set as default = 1). **(H)** Number of *Ptprz1*$^{+/+}$ and *Ptprz1*$^{-/-}$ LMVEC cultured in the presence or absence of crizotinib (mean ± SD, n=3). Two-way ANOVA was used for statistical analysis. **(I)** Migration of *Ptprz1*$^{-/-}$ and *Ptprz1*$^{+/+}$ LMVEC in the presence or absence of crizotinib (mean ± SD). **(J)** Representative photos and quantification of the tube network formed by *Ptprz1*$^{-/-}$ and *Ptprz1*$^{+/+}$ LMVEC on Matrigel, in the presence or absence of crizotinib. Results are expressed as mean ± SD of the percent tube length compared to the solvent-treated *Ptprz1*$^{+/+}$ cells (set as default 100%).

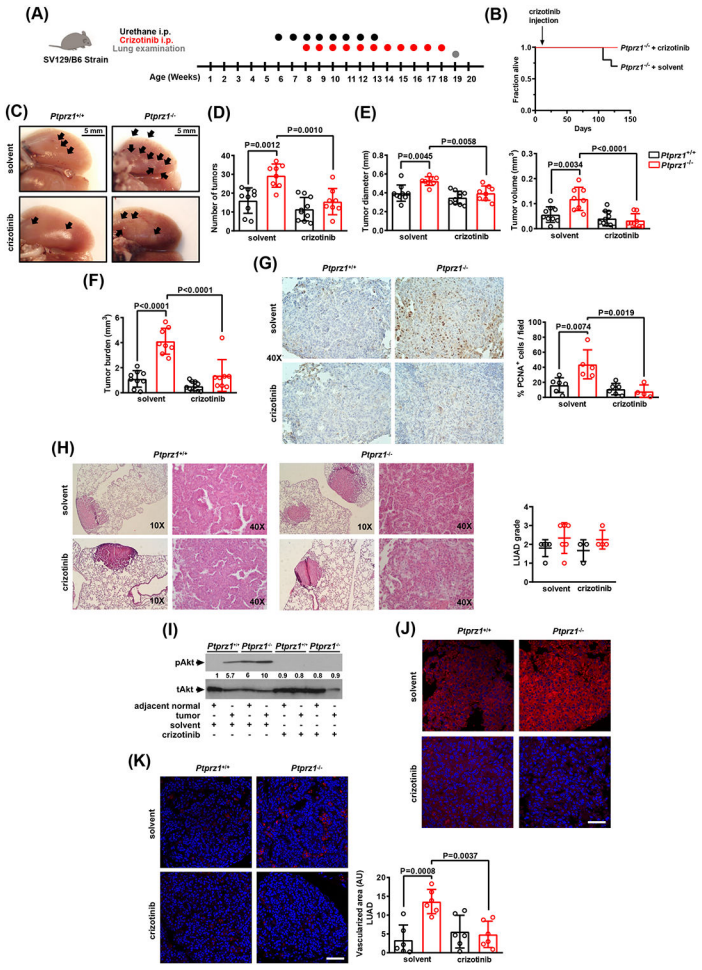

Fig. 4. Crizotinib decreases the enhanced carcinogenesis and tumor angiogenesis observed in *Ptprz1*$^{-/-}$ mice.

(A) Schematic representation of the experimental timeline. **(B)** Kaplan-Meier plot of the survival of the urethane-treated *Ptprz1*$^{-/-}$ mice that received crizotinib or solvent. **(C)** Representative images of the lungs at the end of the experiment. Arrows indicate tumors. The number of tumors per lung **(D),** tumor diameter and volume **(E),** and total tumor burden per lung **(F)** are presented as mean ± SD. **(G)** Representative pictures at 40x magnification of *Ptprz1*$^{-/-}$ and *Ptprz1*$^{+/+}$ tumor tissue sections stained for PCNA (brown) and counterstained by hematoxylin (blue). Results are expressed as mean ± SD of the percent number of PCNA stained (PCNA^{+}) cells per field of tumor tissue. **(H)** Representative pictures from H&E-stained tumor tissue sections at 10x and 40x magnification. The arrows at the 10x magnification point to tumors. Grading of urethane-induced tumors was estimated blindly on a scale from 1 to 5, with 1 indicating the lowest grade. **(I)** Tumors and adjacent normal *Ptprz1*$^{-/-}$ and *Ptprz1*$^{+/+}$ lung tissue lysates from animals treated with crizotinib or solvent were analyzed using antibodies for Akt phosphorylated at Ser473 (pAkt) and total Akt (tAkt). Representative Western blots are shown (n=3). Numbers denote the average fold change of the ratio pAkt/tAkt compared with the adjacent normal *Ptprz1*$^{+/+}$ lung from mice treated with solvent (set as default = 1). **(J)** Paraffin-embedded LUAD tissue sections from animals treated with crizotinib or

solvent are stained for tyrosine phosphorylated c-Met (red). Nuclei are stained with Draq5 (blue). Representative pictures are shown (n=3), and the scale bar corresponds to 50 μm. **(K)** Paraffin-embedded LUAD tissue sections from animals treated with crizotinib or solvent are stained for endothelial cells (red) and nuclei (blue). Representative pictures are shown, and the scale bar corresponds to 50 μm. Results are expressed as mean ± SD of vascularized area per field of LUAD in arbitrary units (AU).

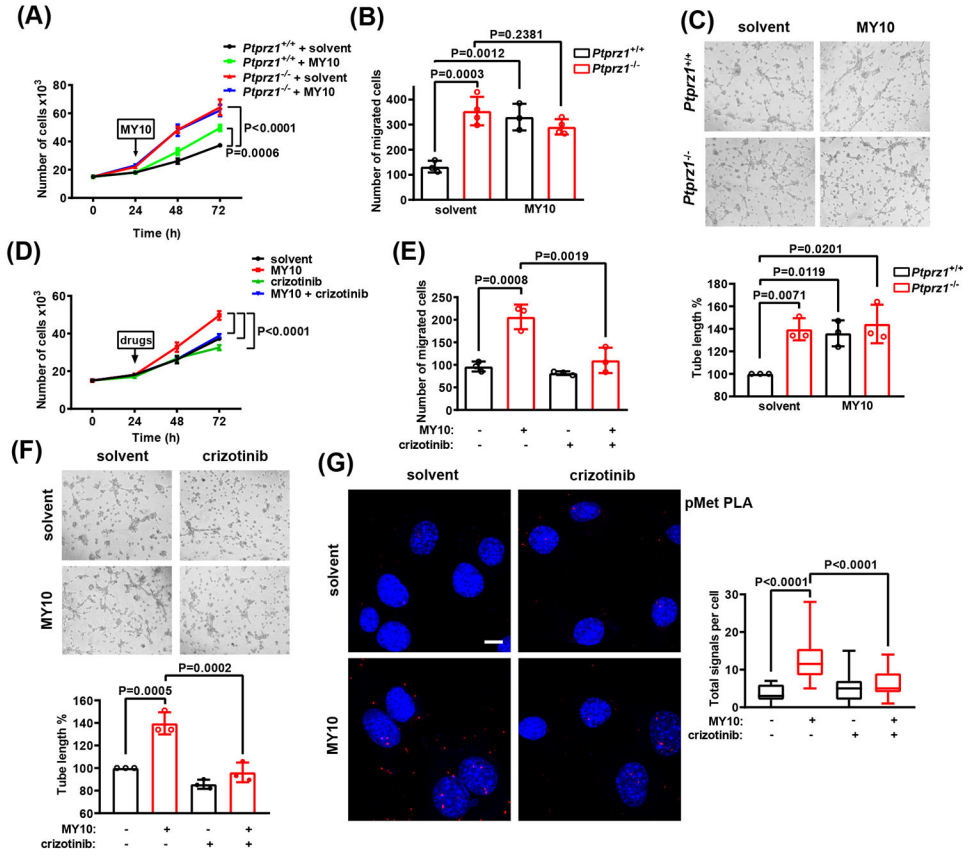

Fig. 5. A selective PTPRZ1 TP inhibitor activates c-Met and enhances angiogenic activities of *Ptprz1*$^{+/+}$ LMVEC in a c-Met-dependent manner.

(A) Numbers of *Ptprz1*$^{-/-}$ and *Ptprz1*$^{+/+}$ LMVEC in the presence or absence of the PTPRZ1 TP inhibitor MY10 (10 μM) (mean ± SD, n=4). Two-way ANOVA was used for statistical analysis. **(B)** Migration of *Ptprz1*$^{-/-}$ and *Ptprz1*$^{+/+}$ LMVEC in the presence or absence of MY10 (mean ± SD). **(C)** Representative photos and quantification of the tube network formed by *Ptprz1*$^{-/-}$ and *Ptprz1*$^{+/+}$ LMVEC in the presence or absence of MY10 on Matrigel. Results are expressed as mean ± SD of the percent tube length compared to the solvent-treated *Ptprz1*$^{+/+}$ cells (set as default 100%). **(D)** The number of *Ptprz1*$^{+/+}$ LMVEC in the presence or absence of MY10 and/or crizotinib (1 μM) (mean ± SD, n=3). Two-way ANOVA was used for statistical analysis. **(E)** Migration of *Ptprz1*$^{+/+}$ LMVEC in the presence or absence of MY10 and/or crizotinib (mean ± SD). **(F)** Representative photos and quantification of the tube network formed by *Ptprz1*$^{+/+}$ LMVECs on Matrigel, in the presence or absence of MY10 and/or crizotinib. Results are expressed as mean ± SD (n=3) of the percent tube length compared to the solvent-treated *Ptprz1*$^{+/+}$ cells (set as default 100%). **(G)** Formation of tyrosine phosphorylated c-Met (pMet) complexes as evidenced by in situ PLA in *Ptprz1*$^{+/+}$ LMVECs cultured in the presence or absence of MY10 and crizotinib. Representative pictures are shown. The scale bar corresponds to 10 μm. The box plots indicate the median, mean, and range of the detected signals (n = 8-10 image fields with 4-6 cells per image per sample type, each sample run in triplicate).

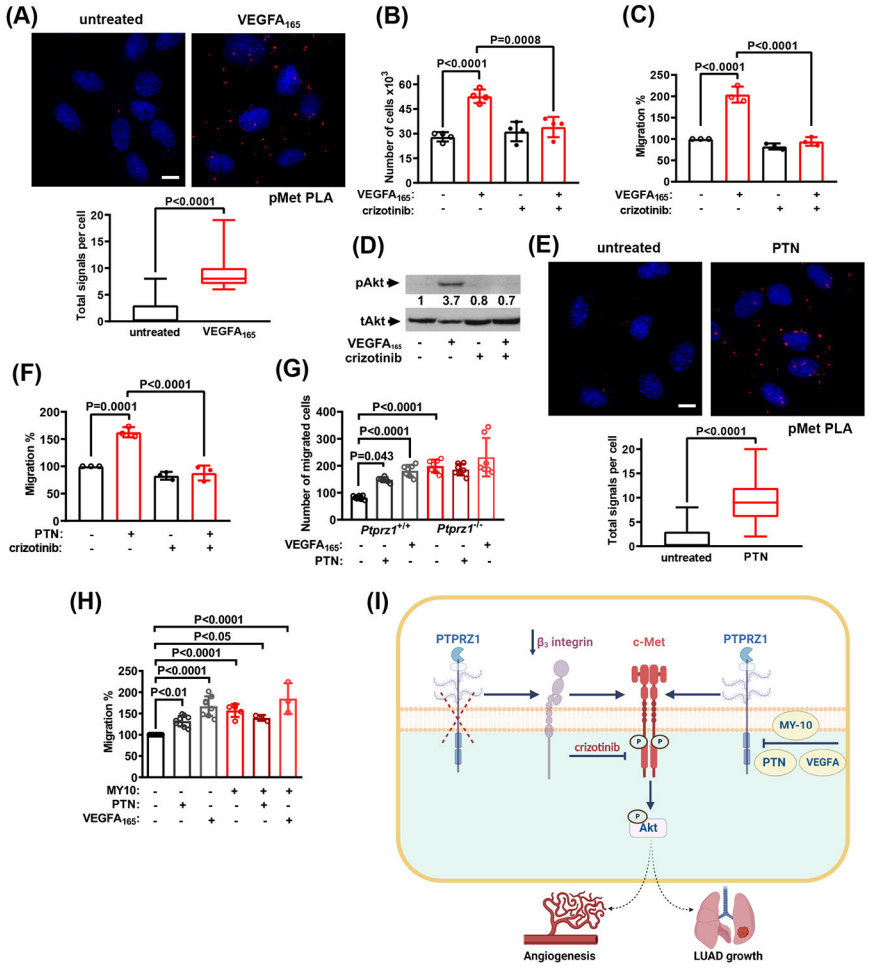

Fig. 6. VEGFA$_{165}$ and PTN activate c-MET through PTPRZ1.

(A) Formation of tyrosine phosphorylated c-Met (pMet) complexes as evidenced by in situ PLA in HUVEC cultured in the presence or absence of VEGFA$_{165}$ (10 ng/ml). Representative pictures are shown. The scale bar corresponds to 10 μm. The box plots indicate the median, mean, and range of the detected signals (n = 8-10 image fields with 4-8 cells per image per sample type, each sample run in triplicate). **(B)** Number of HUVEC in the presence or absence of VEGFA$_{165}$ and/or crizotinib (1 μM) for 24 h (mean ± SD). **(C)** Migration of HUVEC in the presence or absence of VEGFA$_{165}$ and/or crizotinib. Results are expressed as mean ± SD of the percent number of migrated cells compared to the solvent-treated cells (set as default 100%). **(D)** HUVEC were treated with VEGFA$_{165}$ and/or crizotinib and cell lysates were analyzed by antibodies against Akt phosphorylated at Ser473 (pAkt), and total Akt (tAkt). A representative Western blot is shown (n=3). Numbers denote the average fold change of the ratio pAkt/tAkt compared to untreated HUVEC (set as default = 1). **(E)** Formation of tyrosine phosphorylated c-Met (pMet) complexes as evidenced by in situ PLA in HUVEC cultured in the presence or absence of PTN (100 ng/ml). Representative pictures are shown. The scale bar corresponds to 10 μm. The box plots indicate the median, mean, and range of the detected signals (n = 8-10 image fields with 4-8 cells per image per sample type, each sample run in triplicate). **(F)** Migration

of HUVEC in the presence or absence of PTN and/or crizotinib. Results are expressed as mean ± SD of the percent number of migrated cells compared to the solvent-treated cells (set as default 100%). **(G)** Migration of *Ptprz1*$^{-/-}$ and *Ptprz1*$^{+/+}$ LMVEC in the presence or absence of $VEGFA_{165}$ or PTN (mean ± SD). **(H)** Migration of HUVEC in the presence or absence of MY10, stimulated by $VEGFA_{165}$ or PTN. Results are expressed as mean ± SD of the percent number of migrated cells compared to the solvent-treated cells (set as default 100%). **(I) Schematic presentation of the pathway activated by PTPRZ1 deficiency or inhibition in endothelial cells and LUAD.** Deficient PTPRZ1 expression results in β_3 integrin downregulation and activation of c-Met and Akt in endothelial and LUAD cells, leading to activation of endothelial cells, angiogenesis, and LUAD growth (left). VEGFA, PTN, and a specific PTPRZ1 TP inhibitor (MY10) also activate c-Met and Akt in endothelial cells (right). Crizotinib abolishes both LUAD growth and angiogenesis due to low PTPRZ1 expression levels, and the stimulatory effects of VEGFA, PTN, and MY10 on endothelial cell activation. The figure was created with Biorender.